

# Model independent test of the FLRW metric and the curvature in light of DESI DR2

Cléa Millard<sup>ID</sup>,<sup>a</sup> Benjamin L'Huillier<sup>ID</sup>,<sup>a</sup> Marian Douspis<sup>ID</sup><sup>b</sup>

<sup>a</sup>Department of Physics and Astronomy, Sejong University, 05006 Seoul, Republic of Korea

<sup>b</sup>Institut d'Astrophysique Spatiale, Université Paris Saclay & CNRS UMR XXX,

E-mail: [ccm@sju.ac.kr](mailto:ccm@sju.ac.kr), [benjamin@sejong.ac.kr](mailto:benjamin@sejong.ac.kr),  
[marian.douspis@universite-paris-saclay.fr](mailto:marian.douspis@universite-paris-saclay.fr)

**Abstract.** We perform a data-driven test of the FLRW metric and the flatness of the Universe, independently of any Dark Energy model, and in light of the latest DESI DR2 results. We use Pantheon+ and DESY5 SNIa data to reconstruct the distance modulus, dimensionless comoving distance and Hubble parameter, using an iterative smoothing algorithm. Then, combining the various reconstructions with the recent BAO measurements from DESI DR2, we perform the  $\mathcal{O}_k$  diagnostic, a litmus test of the FLRW metric and the flatness of the Universe. We obtain robust results that do not depend on Dark Energy models and test some of the underlying hypotheses of the concordance model. We find that when the reconstructed  $\mathcal{O}_k$  diagnostic is consistent with the FLRW metric, then the median value of  $\Omega_{k,0}$  over all reconstructions that provide an improved fit relative to the flat  $\Lambda$ CDM model are:  $\Omega_{k,0}^{\text{med}} = 0.035_{-0.079}^{+0.046} \pm 0.037$  for the Pantheon+ & DESI DR2 data combination,  $\Omega_{k,0}^{\text{med}} = 0.092_{-0.132}^{+0.055} \pm 0.064$  for the same data but with the Pantheon+ SNIa cut at redshift  $z = 1.13$ , which is the maximum redshift of the DES Y5 data, and  $\Omega_{k,0}^{\text{med}} = -0.119_{-0.047}^{+0.113} \pm 0.043$  for DES Y5 & DESI DR2. The first uncertainties correspond to the spread in  $\Omega_{k,0}$  over all reconstructions, followed by the median  $1\sigma$  error.

ArXiv ePrint: [0000.00000](https://arxiv.org/abs/2601.20293)

---

## Contents

<b>1</b>	<b>Introduction</b>	<b>2</b>
<b>2</b>	<b>Data and method</b>	<b>3</b>
2.1	Litmus test	3
2.2	Data	4
2.3	Iterative smoothing	4
2.4	$\chi^2$ selection criteria	5
<b>3</b>	<b>Results</b>	<b>6</b>
3.1	Smoothing the SNIa	6
3.2	Curvature test	9
<b>4</b>	<b>Discussion and conclusion</b>	<b>13</b>
<b>A</b>	<b>Smoothing scale</b>	<b>15</b>

---

## 1 Introduction

The current concordance model of cosmology, the  $\Lambda$ CDM model, describes a flat universe with an energy budget dominated by dark energy (DE) and cold dark matter (CDM). Since the observation of accelerated expansion using Type Ia supernovae (SNIa) [1, 2], the constraints on the model have been improved by several other probes, among them the cosmic microwave background (CMB, Planck [3]) or the baryon acoustic oscillations (BAO, [4]). However, despite its success, some tensions have arisen in the  $\Lambda$ CDM model, especially in determining the value of the Hubble constant  $H_0$ . To this day, the late-type direct measurements of  $H_0$  remain in tension with the early-time inferences (for a given model e.g.  $\Lambda$ CDM) at a  $> 3\sigma$  level [5]. To resolve this tension, numerous alternative DE models have been suggested [6] but with limited success. Recently, the second data release of the Dark Energy Spectroscopic Instrument (DESI) hinted significantly at a dynamical DE equation of state, shaking the cosmological constant model from  $\Lambda$ CDM.

In addition to parametric fits of alternative models, model-independent reconstructions of the expansion history of the Universe allow to directly test the consistency of the data with the assumptions underlying these models. In particular, one of the most fundamental assumption underlying the  $\Lambda$ CDM model is that the Universe is homogeneous and isotropic. This assumption is encoded into the Friedmann–Lemaître–Robertson–Walker (FLRW) metric, in which the expansion history of the Universe is governed by the following equation:

$$h(z) = \sqrt{\Omega_{\text{m},0}(1+z)^3 + \Omega_{k,0}(1+z)^2 + \Omega_{\text{DE},0} \exp\left(3 \int_0^z \frac{1+w(z')}{1+z'}\right)} \quad (1.1)$$

where  $w(z) = P/\rho$  is the equation of state of DE,  $\Omega_{\text{m},0}, \Omega_{k,0}, \Omega_{\text{DE},0}$  are the density parameter of matter, curvature, and DE today. Then, the dimensionless comoving distance of an astronomical object is, for all signs of  $\Omega_{k,0}$ :

$$\mathcal{D}(z) = \frac{1}{\sqrt{-\Omega_{k,0}}} \sin\left(\sqrt{-\Omega_{k,0}} \int_0^z \frac{dz'}{h(z')}\right), \quad (1.2)$$

which is related to the luminosity distance  $d_{\text{L}}(z)$  and the comoving distance  $d_{\text{M}}$  by:

$$\frac{c}{H_0} \mathcal{D}(z) = d_{\text{M}}(z) = \frac{d_{\text{L}}(z)}{1+z}. \quad (1.3)$$

The distance modulus of type Ia supernovae is directly linked to the luminosity distance by:

$$\mu(z) = 5 \log_{10} \left( \frac{d_{\text{L}}(z)}{1 \text{ Mpc}} \right) + 25, \quad (1.4)$$

so that:

$$\mathcal{D}(z) = \frac{H_0}{c} \frac{10^{\frac{\mu(z)}{5}-5}}{1+z} \times 1 \text{ Mpc}. \quad (1.5)$$

In the case of a flat universe ( $\Omega_{k,0} = 0$ ), the dimensionless comoving distance becomes:

$$\mathcal{D}(z) = \int_0^z \frac{dz'}{h(z')}. \quad (1.6)$$

The transverse and radial modes of the BAO data provide the ratio of the comoving distance  $d_{\text{M}}$  and of the Hubble distance  $d_{\text{H}} = c/H_0$  to the sound horizon at drag epoch  $r_{\text{d}}$ .

In the search for beyond  $\Lambda$ CDM physics, it is important to establish null tests of these underlying assumptions. The goal of model-independent null test of the FLRW metric is to detect deviations from FLRW that would indicate a break from the usual homogeneity and anisotropy assumption, and this without assuming any DE model. In this work, we use the  $\mathcal{O}_k$  diagnostic [7, 8], a litmus test of the FLRW metric and the spatial curvature. We reconstruct the  $\mathcal{O}_k$  diagnostic using a combination of BAO data from DESI DR2 and model-independent reconstructions of the dimensionless distance of SNIa from Pantheon+ or the Dark Energy Survey (DES) Y5. The methodology is taken from [9–11]. Additional model-independent null tests of the FLRW metric have been performed using SNIa and BAO data [12], BAO DESI DR2 data alone [13], and strong-lensing time-delay observations [14]. The advantage of our combined dataset, model-independent approach, is that the results of the litmus test do not depend on the values of  $H_0$  and  $r_d$ . We also introduce a p-value test to define which reconstructions of the  $\mathcal{O}_k$  diagnostic are consistent with the FLRW metric, and for which the value of  $\mathcal{O}_k$  can be interpreted as  $\Omega_{k,0}$ . The paper is organised as follow: Section 2 describes the methods and data used to construct the  $\mathcal{O}_k$  test, the p-value test and the results are presented in Section 3 and discussion takes place in Section 4.

## 2 Data and method

### 2.1 Litmus test

The  $\mathcal{O}_k$  diagnostic [7, 8] is a litmus test for the FLRW metric. It is defined as :

$$\mathcal{O}_k(z) = \frac{\Theta^2(z) - 1}{\mathcal{D}^2(z)}, \quad (2.1a)$$

$$\Theta(z) = h(z)\mathcal{D}'(z) = \sqrt{1 + \Omega_{k,0}\mathcal{D}^2(z)}, \quad (2.1b)$$

where ' denotes differentiation with respect to redshift. In an FLRW universe,  $\mathcal{O}_k$  is constant such as  $\mathcal{O}_k(z) \equiv \Omega_{k,0}$ , so we expect  $\mathcal{O}_k = 0$  if this universe is also flat. If a deviation from  $\mathcal{O}_k(z) = \text{cst}$  is observed, it is an indication that the data might not be consistent with the FLRW metric.

According to [9–11], the quantity  $c/(H_0 r_d)$  can be computed using two methods:

$$\frac{c}{H_0 r_d} = \frac{1}{\mathcal{D}(z)} \frac{d_M(z)}{r_d} \quad (2.2a)$$

$$\frac{c}{H_0 r_d} = h(z) \frac{c}{H(z)r_d}. \quad (2.2b)$$

In a flat FLRW universe, equation (2.2b) becomes:

$$\frac{c}{H_0 r_d} = \frac{1}{\mathcal{D}'(z)} \frac{d_H(z)}{r_d}, \quad (2.2c)$$

and the parameter  $\Theta$  can be re-written as the ratio between the two methods:

$$\Theta(z) = \frac{d_M(z)/r_d}{d_H(z)/r_d} \frac{\mathcal{D}'(z)}{\mathcal{D}(z)}. \quad (2.3)$$

Using equations (2.1a) and (2.3), we can reconstruct the  $\mathcal{O}_k$  diagnostic using BAO data (providing  $d_M/r_d$  and  $d_H/r_d$ ) and model-independently reconstructed  $\mathcal{D}$  and  $\mathcal{D}'$  from SNIa data, at the redshift of the BAO.

## 2.2 Data

To construct the  $\mathcal{O}_k$  diagnostic we use the transverse and radial modes of DESI DR2 BAO data within the redshift range covered by the SNIa data. These quantities are obtained from the clustering of galaxies measured by DESI, through the analysis of the two-point correlation function of the galaxy distribution. The BAO data points and their correlations are taken from [4], Table IV. The redshift bins are uncorrelated, however, we take into account the correlation between the transverse and radial modes. We note that, while the measurement  $d_M/r_d$  does not assume flatness, a flat FLRW universe is assumed in the whole BAO pipeline. Additionally, we use two compilations of Type Ia supernovae (SNIa): Pantheon+ and DES Y5, from which we will reconstruct  $\mathcal{D}$  and  $\mathcal{D}'$ . The Pantheon+ sample consists of 1550 spectroscopically confirmed SNIa, spanning a redshift 0.001 to 2.26 [15]. In contrast, DES Y5 compiles 1829 SNIa within  $0.10 < z < 1.13$  [16]. When combining the DESI DR2 BAO data with Pantheon+, we use the five BAO points comprised in  $0.510 < z < 1.484$ , as to not exceed the maximum redshift of the SNIa compilation. For the same reason, we only use three BAO data points such as  $0.510 < z < 0.934$  when combining them with DES Y5.

## 2.3 Iterative smoothing

The distance moduli of SNIa can be reconstructed through the non-parametric method of iterative smoothing [17, 18]. This method allows us to estimate  $\mathcal{D}$  and  $\mathcal{D}'$  at arbitrary redshift, particularly at the redshift of the BAO, a necessary estimation to reconstruct the  $\mathcal{O}_k$  diagnostic (see eq. (2.3)). It is also independent of any DE model, allowing a model-independent estimation of the value of  $\mathcal{O}_k$  at the BAO redshifts. The distance modulus  $\hat{\mu}(z)$  is reconstructed directly from an initial guess  $\hat{\mu}_0(z)$ , using a data set  $\{z_i, \mu_i\}$  with a covariance matrix  $\mathbf{C}_{\text{SNIa}}$ . At each iteration  $n + 1$ , a Gaussian kernel with a smoothing scale  $\Delta$  smooths the residuals  $\delta\mu_n$  between the data and the reconstruction  $n$ :

$$\hat{\mu}_{n+1}(z) = \hat{\mu}_n(z) + \frac{\mathbf{W}^\top(z) \mathbf{C}_{\text{SNIa}}^{-1} \delta\mu_n}{\mathbf{W}^\top(z) \mathbf{C}_{\text{SNIa}}^{-1} \mathbf{1}}, \quad (2.4)$$

where the weights  $\mathbf{W}$  and the residuals  $\delta\mu_n$  are defined as:

$$[\mathbf{W}(z)]_i = \exp\left(-\frac{\ln^2\left(\frac{1+z}{1+z_i}\right)}{2\Delta^2}\right), \quad (2.5)$$

$$[\delta\mu_n]_i = \mu_i - \hat{\mu}_n(z_i). \quad (2.6)$$

The smoothing scale determines the weight that a data point will have in the smoothing depending on its distance from the test point  $z$ . The larger  $\Delta$ , the more influence the distant data point will have on the smoothing. We will use  $\Delta = 0.3$ , in accordance with previous studies [9, 10, 17–22]. This value was originally used in [8] for a sample of 397 SNIa. Regardless of the initial guess, successive reconstructions will converge toward the same result [9, 10, 17, 18]. The final collection of reconstructions forms a non-exhaustive set of plausible expansion histories.

From the collection of reconstructed distance moduli  $\{\hat{\mu}_n(z)\}$ , we can obtain the collection of reconstructed dimensionless distances  $\{\hat{\mathcal{D}}_n(z)\}$ . Their smoothed derivative  $\{\hat{\mathcal{D}}'_n(z)\}$  is also obtained by smoothing, as described in [11]. The reconstructed  $\hat{\mathcal{D}}_n$  and  $\hat{\mathcal{D}}'_n$  must be normalized to ensure  $\hat{\mathcal{D}}'_n(z=0) = 1$ .

## 2.4 $\chi^2$ selection criteria

As explained in section 2.1, we can now combine the reconstructed  $\{\widehat{\mathcal{D}}_n\}$  and  $\{\widehat{\mathcal{D}}'_n\}$  with the BAO measurements to calculate the  $\mathcal{O}_k$  diagnostic. For each reconstruction, three different  $\chi^2$  can be considered :

1. The  $\chi^2$  to the SNIa data alone:

$$\delta\boldsymbol{\mu} = \widehat{\mu}_n(\mathbf{z}_{\text{SNIa}}) - \boldsymbol{\mu}, \quad (2.7a)$$

$$\chi_{\text{SNIa}}^2 = \delta\boldsymbol{\mu}^\top \mathbf{C}_{\text{SNIa}}^{-1} \delta\boldsymbol{\mu}, \quad (2.7b)$$

where  $\mathbf{z}_{\text{SNIa}}$  and  $\boldsymbol{\mu}$  are of dimension  $N_{\text{SNIa}}$ , the total number of SNIa in the sample.

2. The  $\chi^2$  to the SNIa and the transverse mode of the BAO  $d_{\text{M}}/r_{\text{d}}$ :

$$\delta\mathbf{y}_{\text{M}} = \theta_{\text{M},n} \widehat{\mathcal{D}}_n(\mathbf{z}_{\text{BAO}}) - \frac{\mathbf{d}_{\text{M}}}{\mathbf{r}_{\text{d}}}, \quad (2.8a)$$

$$\chi_{\text{SNIa}+d_{\text{M}}}^2 = \chi_{\text{SNIa}}^2 + \delta\mathbf{y}_{\text{M}}^\top \mathbf{C}_{d_{\text{M}}/r_{\text{d}}}^{-1} \delta\mathbf{y}_{\text{M}}, \quad (2.8b)$$

where

$$\theta_{\text{M},n} = \frac{\mathbf{1}^\top \mathbf{C}_{d_{\text{M}}/r_{\text{d}}} \left. \frac{\mathbf{c}}{H_0/r_{\text{d}}} \right|_n}{\mathbf{1}^\top \mathbf{C}_{d_{\text{M}}/r_{\text{d}}} \mathbf{1}} \quad (2.9)$$

is the weighted average over the values of  $\mathbf{c}/(H_0 r_{\text{d}})$  computed at each BAO redshift during iteration  $n$  following eq. (2.2a), and contained in the vector  $\left. \frac{\mathbf{c}}{H_0/r_{\text{d}}} \right|_n$  of dimension  $N_{\text{BAO}}$ , the number of BAO measurements.  $\mathbf{z}_{\text{BAO}}$  and  $\frac{\mathbf{d}_{\text{M}}}{\mathbf{r}_{\text{d}}}$  are also vectors of dimension  $N_{\text{BAO}}$ , and  $\mathbf{C}_{d_{\text{M}}/r_{\text{d}}}^{-1}$  is the (diagonal) inverse covariance matrix of the transverse BAO mode.

3. The  $\chi^2$  to both SNIa and the complete BAO data:

$$\delta\mathbf{y}_{\text{H}} = \theta_{\text{H},n} \widehat{\mathcal{D}}'_n(\mathbf{z}_{\text{BAO}}) - \frac{\mathbf{d}_{\text{H}}}{\mathbf{r}_{\text{d}}}, \quad (2.10a)$$

$$\chi_{\text{tot}}^2 = \begin{pmatrix} \delta\mathbf{y}_{\text{M}} \\ \delta\mathbf{y}_{\text{H}} \end{pmatrix}^\top \mathbf{C}_{\text{BAO}}^{-1} \begin{pmatrix} \delta\mathbf{y}_{\text{M}} \\ \delta\mathbf{y}_{\text{H}} \end{pmatrix}, \quad (2.10b)$$

where  $\mathbf{C}_{\text{BAO}}^{-1}$  is the inverse covariance matrix of the BAO measurements, and  $\theta_{\text{H},n}$  is computed similarly to eq. (2.9), where  $\mathbf{c}/(H_0 r_{\text{d}})$  is calculated via eq. (2.2c). It is important to note that this equation assumes flatness.

From there, we define :

$$\Delta\chi_{\text{data}}^2 = \chi_{\text{data}}^2 - \chi_{\text{data,f}\Lambda\text{CDM}}^2 \quad (2.11)$$

where the data considered for the fit are one of the three configurations described above (eq. 2.7a, 2.8a and 2.10a) and  $\chi_{\text{data,f}\Lambda\text{CDM}}^2$  is the  $\chi^2$  of the flat  $\Lambda\text{CDM}$  model that best fits these data. The function  $\chi_{\text{data,f}\Lambda\text{CDM}}^2(\Omega_{\text{m},0}, M_{\text{B}})$  was minimised with fixed  $H_0 = 67.66 \text{ km s}^{-1} \text{ Mpc}^{-1}$  (taken from Planck 2018 [3]) and  $M_{\text{B}}$  the absolute magnitude of SNIa treated as a nuisance parameter. In the following, we will apply the selection criteria  $\Delta\chi_{\text{data}}^2 < 0$ , so that we only use the reconstructions with a better fit to the data than the best fitting flat  $\Lambda\text{CDM}$ . Using the selection criteria  $\Delta\chi_{\text{tot}}^2 < 0$  filters out reconstructions inconsistent with flatness. Such a selection can be used as a self consistency check of the  $\mathcal{O}_k$  diagnostic, but the results should not be used as a genuine litmus test of the FLRW metric and flatness.

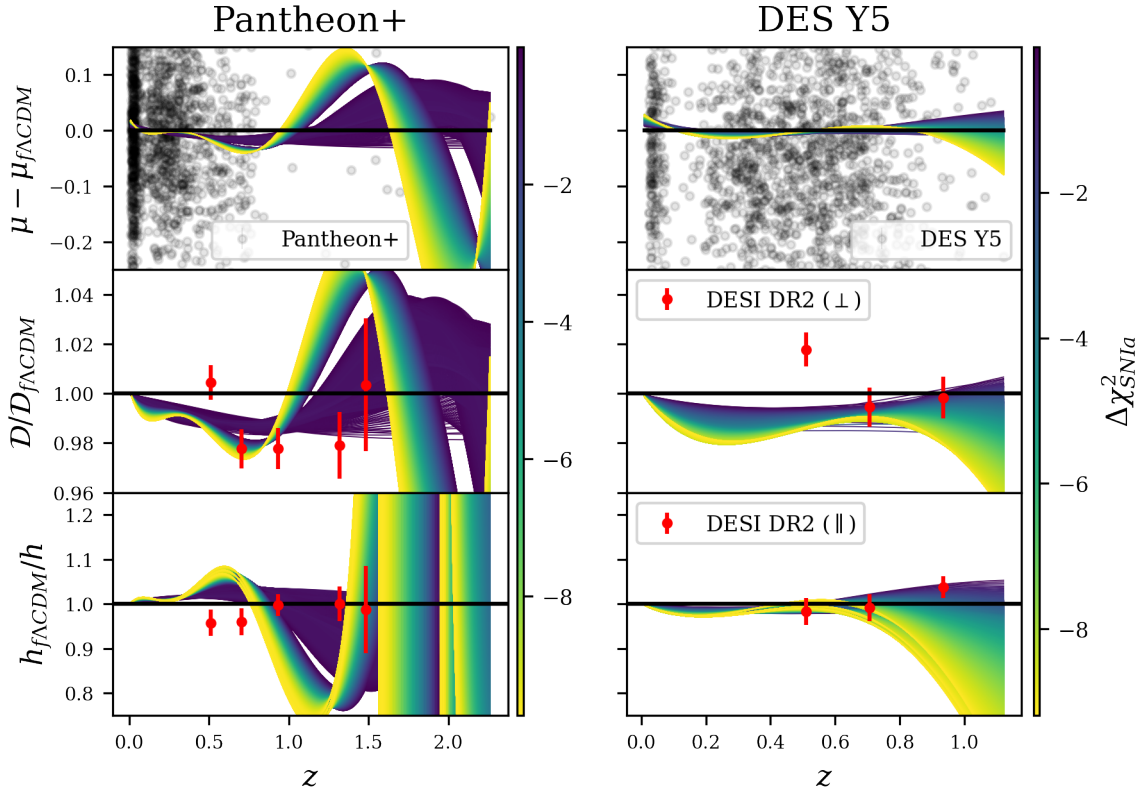


**Figure 1:** Iterative smoothing on SNIa data. The results for the Pantheon+ compilation are displayed in the left column, while the results for DES Y5 are displayed in the right column. The selection criterion is  $\Delta\chi^2_{\text{SNIa}} < 0$ , and the reconstructions are colour-coded by  $\Delta\chi^2_{\text{SNIa}}$ . The **top row** shows the results in the residual space  $\mu(z) - \mu_{\text{f}\Lambda\text{CDM}}(z)$ , the **middle row** shows the dimensionless comoving distance  $\mathcal{D}(z)$  of eq. (1.5) normalised by  $\mathcal{D}_{\text{f}\Lambda\text{CDM}}(z)$ , and the **bottom row** displays the normalised dimensionless Hubble parameter from eq. (1.6). The subscript  $\text{f}\Lambda\text{CDM}$  indicates a quantity derived from the flat  $\Lambda\text{CDM}$  model that best fits the SNIa data.

### 3 Results

#### 3.1 Smoothing the SNIa

We perform the iterative smoothing algorithm on both Pantheon+ and DES Y5 dataset. Various flat  $\Lambda\text{CDM}$  cosmologies are used as initial guesses. The upper row of Figure 1 shows the results of the iterative smoothing of the distance modulus for the selection criterion  $\Delta\chi^2_{\text{SNIa}} < 0$ . The selected reconstructions are colour-coded by  $\Delta\chi^2_{\text{SNIa}}$ . The left column shows the results of the iterative smoothing on Pantheon+ SNIa, while the right column shows the results for DES Y5. The results are plotted in the residual space  $\mu(z) - \mu_{\text{f}\Lambda\text{CDM}}(z)$ , where  $\mu_{\text{f}\Lambda\text{CDM}}$  is the distance modulus of the flat  $\Lambda\text{CDM}$  cosmology that best fits the data. In the second row are the reconstructions of the dimensionless luminosity distance  $\mathcal{D}$  normalized by the best fit  $\mathcal{D}_{\text{f}\Lambda\text{CDM}}$ , using eq. (1.5). Finally, in the third row, we display the inverse of the normalized Hubble parameter  $h_{\text{f}\Lambda\text{CDM}}/h$ , under the assumption that  $\Omega_{k,0} = 0$  (see eq. 1.6). For information purposes, we over-plotted the BAO data from DESI DR2 in the two bottom

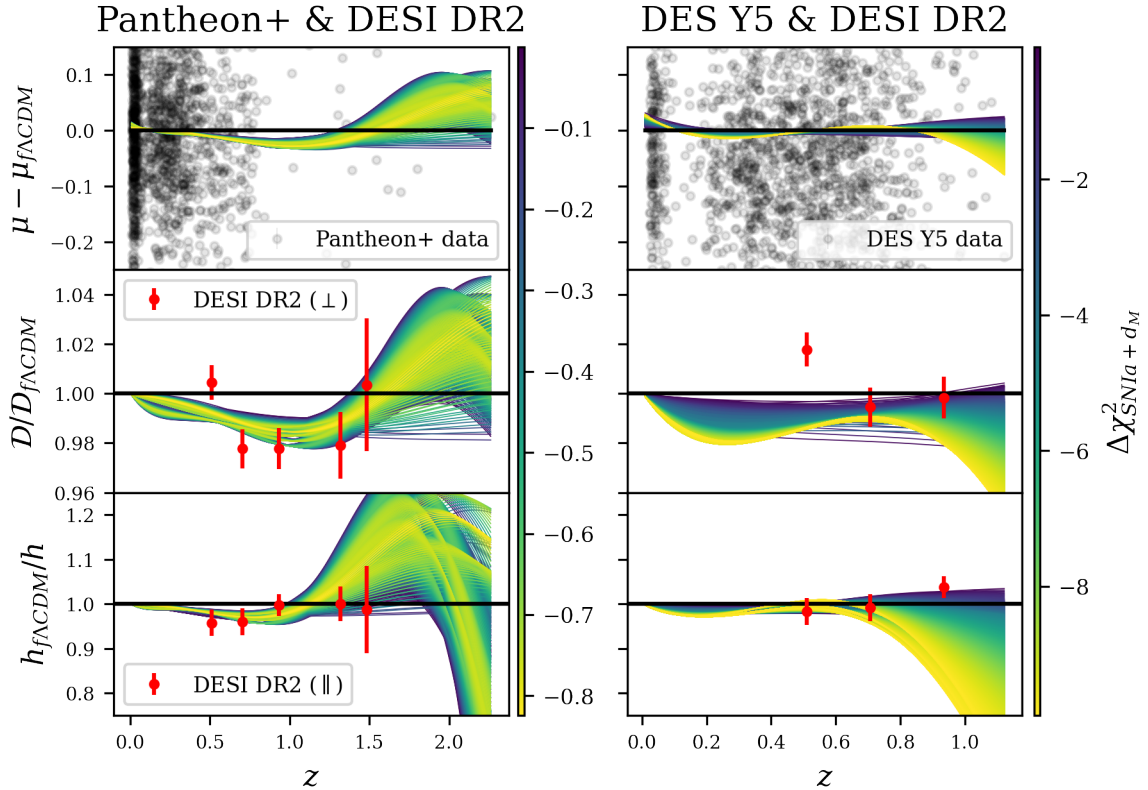


**Figure 2:** Same as Fig. 1, but using selection criterion  $\Delta\chi^2_{\text{SNIa}+d_M} < 0$

rows of the figures, but we emphasize that they were not involved in smoothing. The  $c/(H_0 r_d)$  value used to plot the BAO data in the two bottom panels is taken from Planck 2018 [3]. The Pantheon+ reconstructions that best fit the SNIa data (in yellow) appear to be those that fit the less the BAO data, plotted in red in the two bottom rows. At high redshift, where the data become sparse, the reconstructions strongly deviate from the best-fitting flat  $\Lambda\text{CDM}$ .

When changing the selection criterion to  $\Delta\chi^2_{\text{SNIa}+d_M} < 0$  in the left column of Fig. 2, we can see, as expected, that the reconstructions that best fit the SNIa data in Fig. 1 are left out. In the second row of the left column, we can see that the remaining reconstructions have a good fit to the transverse BAO data point. Adding information from the transverse BAO mode strongly affect the Pantheon+ collection of selected reconstructions. This can be seen in the left panel of Fig. 3, which shows the evolution of  $\Delta\chi^2_{\text{data}}$  for the three considered selection criteria. Each solid line corresponds to one choice of initial condition. The blue solid lines show the evolution of  $\Delta\chi^2_{\text{SNIa}}$ . Similarly, the red lines correspond to the evolution of  $\Delta\chi^2_{\text{SNIa}+d_M}$  and the green lines to  $\Delta\chi^2_{\text{tot}}$ . As expected,  $\Delta\chi^2_{\text{SNIa}}$  (in blue) becomes more and more negative as the iterative smoothing progresses and the smooth reconstructions get closer to the data for both Pantheon+ and DES Y5. In the case of DES Y5, the reconstructed comoving distances are also in good agreement with the transverse BAO mode, leading to a slightly lower  $\Delta\chi^2_{\text{SNIa}+d_M}$ . However, the disagreement between the reconstructed distances from Pantheon+ and the comoving distances from DESI DR2 can be seen in the red lines of the left panel. In this case,  $\Delta\chi^2_{\text{SNIa}+d_M}$  first decreases during the first few iterations, and then starts increasing and diverges away from zero.

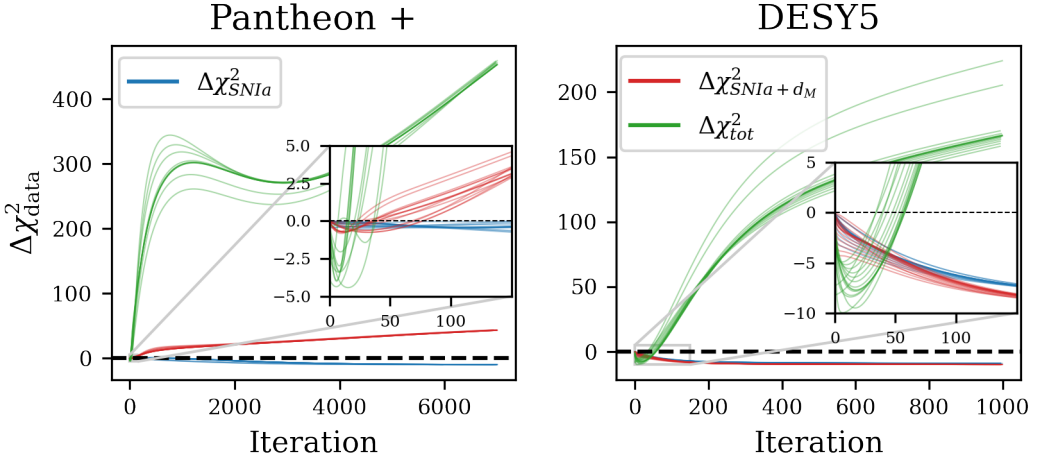


**Figure 3:** Iterative evolution of  $\Delta\chi^2_{\text{data}}$ . The blue curves are the goodness of fit of the reconstruction to the SNIa data alone, the red curves to both SNIa and the transverse BAO mode, and the green curves to both the SNIa and the complete BAO data. The various curves of same colour correspond to different initial guesses. The black dotted horizontal line represents the selection criterion. Reconstruction crossing into  $\Delta\chi^2_{\text{data}} > 0$  will not be kept for the  $\mathcal{O}_k$  diagnostic.

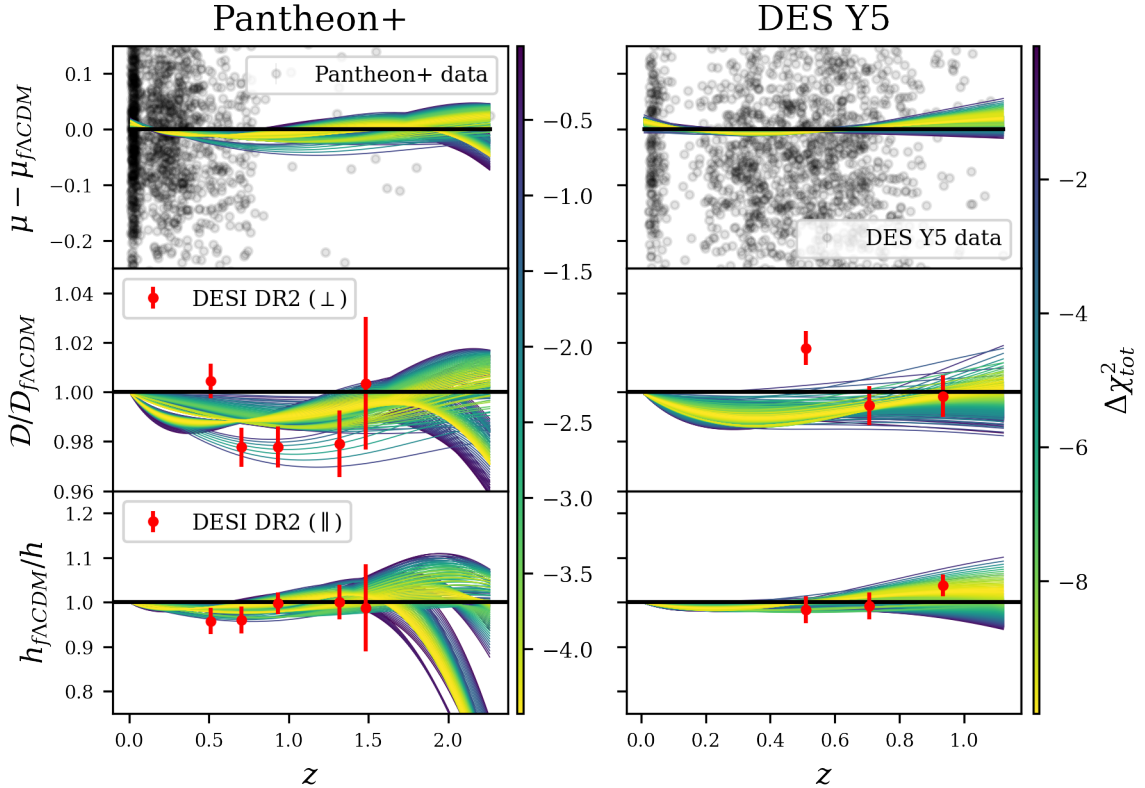


**Figure 4:** Same as Fig. 1, but using selection criterion  $\Delta\chi^2_{\text{tot}} < 0$

This reveals a tension between the Pantheon+ and the DESI DR2 data : the Pantheon+ data, which become sparse at redshift  $z > 1$ , drive the reconstructions away from the BAO data. This is not the case for the DES Y5 collection: even if  $\Delta\chi_{\text{SNIa}+d_M}^2 > \Delta\chi_{\text{SNIa}}^2$ ,  $\Delta\chi_{\text{SNIa}+d_M}^2$  does not cross into positive values. Consequently, the DES Y5 collection remains virtually unchanged under the new selection criterion.

Finally, in Figure 4 the selection criterion  $\Delta\chi_{\text{tot}}^2 < 0$  was applied. Following the considerations of the end of section 2.4, the selected reconstructions are the ones that agree best with both modes of the BAO, illustrating that this selection criterion favours expansion histories consistent with a flat universe. This comes from the definition of  $d_H/r_d$  in eq. (2.2c), which is involved in the computation of  $\Delta\chi_{\text{tot}}^2$  via eq. (2.10a) and assumes flatness.

### 3.2 Curvature test

The results for the reconstruction of the  $\mathcal{O}_k$  diagnostic using the reconstructions of Fig. 1, are displayed in Fig. 5, where the selection criterion applied is  $\Delta\chi_{\text{SNIa}}^2 < 0$ . In order not to overload the plot and help readability, only 500 reconstructions were plotted among the complete collection of selected reconstructions. To ensure that the plotted sample represents the diversity of results, the 500 hundred plotted reconstructions were sampled uniformly in  $\Delta\chi_{\text{SNIa}}^2$ . The left column shows the  $\mathcal{O}_k$  diagnostic for each reconstruction, with its  $1\sigma$  uncertainty, propagated as indicated in [11]. Note that the error bars are higher at lower redshift due to the division by  $\mathcal{D}(z)^2$  during error propagation). The results were calculated at the BAO redshifts, but for readability, each reconstruction is plotted with a distinct offset in  $z$ . The right column shows the likelihoods  $\mathcal{L} = \exp(-\chi_{\mathcal{O}_k}^2/2)$  of each reconstruction, where  $\chi_{\mathcal{O}_k}^2$  is the  $\chi^2$  of a constant to the  $\mathcal{O}_k$  diagnostic. As previously, the reconstructions are colour-coded by  $\Delta\chi_{\text{SNIa}}^2$ . The first row displays the results for the combination of Pantheon+ & DESI DR2. In the middle row, we restrict the redshift range to the 3 lowest BAO redshifts. Finally, the results for DESY Y5 & DESI DR2 are displayed in the bottom row.

In the Pantheon+ & DESI DR2 case, the reconstructions with more negative  $\Delta\chi_{\text{SNIa}}^2$  (in yellow), which are the most favoured by the (SN) data, appear to deviate significantly from constant, and thus from FLRW, at high redshift. Their corresponding likelihoods have indeed a very low peak, especially when compared to the likelihoods of reconstructions with less negative  $\Delta\chi_{\text{SNIa}}^2$  (in violet). These reconstructions, having a  $\Delta\chi_{\text{SNIa}}^2$  close to zero, provide a comparatively poorer fit to the data, but their high-peaked likelihood indicate a far better consistency with the FLRW metric. When reconstructions are inconsistent with the FLRW metric, the  $\mathcal{O}_k$  diagnostic cannot be extended as a test on curvature. Consequently, we decide to filter out the reconstructions that are inconsistent with FLRW before moving into the curvature test. To do so, we perform a  $p$ -value test on the collection of reconstructions. We assume that  $\chi_{\mathcal{O}_k}^2$  follows a  $\chi^2_\nu$  distribution of degree of freedom  $\nu = N_{\text{BAO}} - p$ , where  $N_{\text{BAO}}$  is the number of BAO data points and  $p = 1$  is the number of parameters in the model (here, the model is a constant fitting). We choose  $\alpha = 0.05$ , and reject all reconstructions with  $p < \alpha$ , so that we can affirm with 95% confidence that the reconstructions that pass the test are consistent with a constant  $\mathcal{O}_k$ , and that this  $\mathcal{O}_k$  can be interpreted as an estimation of  $\Omega_{k,0}$ . In Table 1 we report  $\Omega_{k,0}^{\text{med}}$  the median of these constants  $\Omega_{k,0}$ , with the spread of all FLRW-consistent reconstructions  $\Delta\Omega_{k,0} = \max\Omega_{k,0} - \min\Omega_{k,0}$ , and the median  $1\sigma$  errors  $\sigma_{\Omega_{k,0}^{\text{med}}}$ , as well as the median value of  $c/(H_0 r_d)$  computed with eq. (2.2a). Our various estimations of  $c/H_0 r_d$  are all consistent within  $2\sigma$  with the value from Planck 2018  $c/H_0 r_d = 30.26 \pm 0.28$  [3].

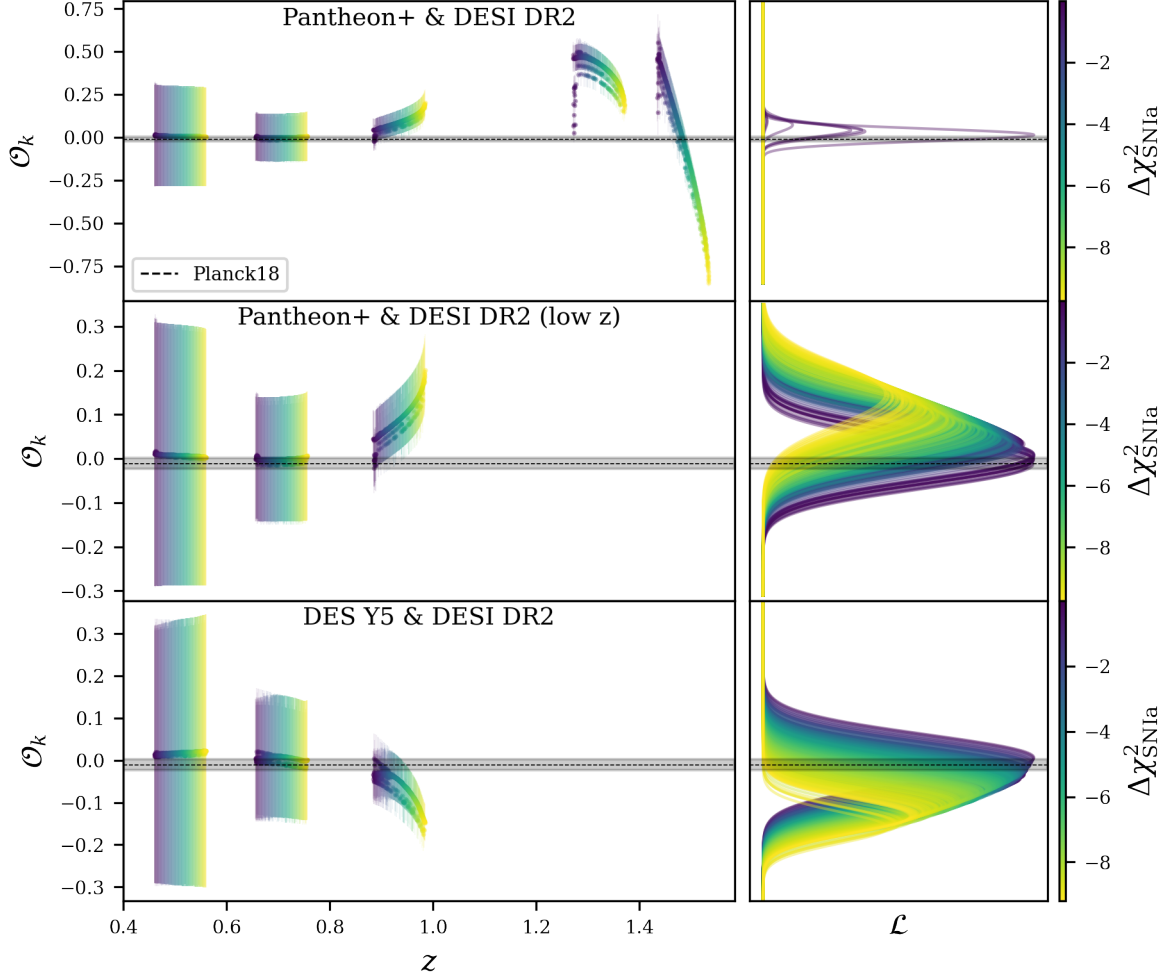


**Figure 5:** Results for the  $\mathcal{O}_k$  diagnostic, with selection criterion  $\Delta\chi^2_{\text{SNIa}} < 0$ . From top to bottom are displayed the results for the combination of Pantheon+ & DESI DR2, Pantheon+ & DESI DR2 truncated at  $z = 1.13$  and DES Y5 & DESI DR2. **Left column:**  $\mathcal{O}_k$  diagnostic of each selected reconstructions at the redshift of the DESI DR2 BAO, along with their  $1\sigma$  errors and colour-coded by  $\Delta\chi^2_{\text{SNIa}}$ . For readability purpose, the result of each reconstruction is plotted with a slight, distinct offset in  $z$  around the original BAO redshift. **Right column:** likelihoods of each reconstruction, colour-coded by  $\Delta\chi^2_{\text{SNIa}}$ .

Only 1.12% the Pantheon+ & DESI DR2 reconstructions pass the  $p$ -value test. The remaining reconstructions are consistent with the FLRW metric, with  $\Omega_{k,0}^{\text{med}} = 0.058^{+0.043}_{-0.107} \pm 0.038$ , where the first uncertainty is the spread of the central value of  $\Omega_{k,0}$  over all the reconstructions, and the second uncertainty is the median of the  $1\sigma$  uncertainties (see Table 1). The maximum deviation from flatness is  $2.55\sigma$ , while maintaining a slight preference for positive curvature. When considering only the lower redshift range ( $z < 1.13$ ) for the BAO data to protect the  $\mathcal{O}_k$  diagnostic from edge effects and the sparsity of high- $z$  Pantheon+ data, 100% of the reconstructions are consistent with FLRW, supporting the conclusion that the deviation from FLRW in the Pantheon+ & DESI DR2 data combination is driven by the high redshift supernovae. The reconstructions best-fitting the SNIa still present a lower likelihood, and they drive  $\Omega_{k,0}$  away from flatness and toward positive values. The median

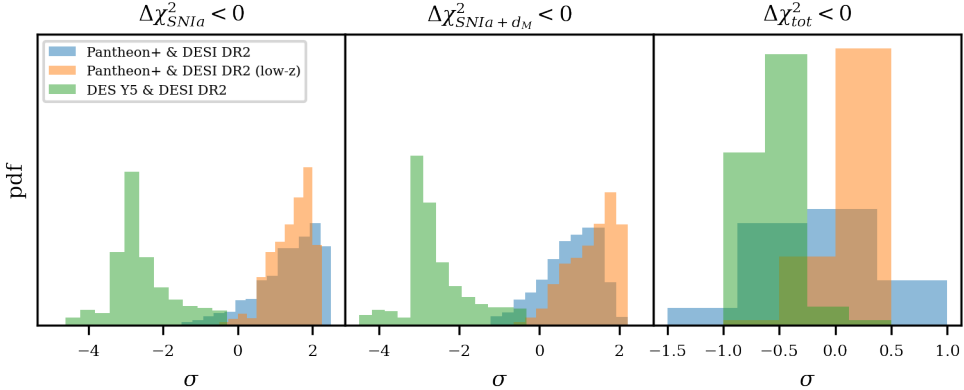


**Figure 6:** For each selection criterion, histogram of the deviation from flatness of the reconstructions that passed the  $p$ -value test and are therefore consistent with the FLRW metric.

value is  $\Omega_{k,0}^{\text{med}} = 0.098_{-0.134}^{+0.048} \pm 0.064$ , with a maximum deviation from flatness of  $2.13\sigma$ .

On the contrary, DES Y5 & DESI DR2 have an excellent consistency with the FLRW metric. Indeed, this combination of data results in 100% of the reconstructions passing the  $p$ -value test. The median constant is  $\Omega_{k,0}^{\text{med}} = -0.119_{-0.047}^{+0.125} \pm 0.043$  with a maximum deviation from flatness of  $-4.44\sigma$ , which correspond to reconstructions with the best fit to the SNIa data (in yellow). However, we can see on the left panel of Fig. 6 that most reconstructions remains consistent with flatness within  $3\sigma$ . Similarly to the Pantheon+ & DESI DR2 (low- $z$ ) results, these reconstructions best fitting the DES Y5 SNIa (in yellow) tend to have a lower likelihood and are centered around higher  $\mathcal{O}_k$  than the reconstruction with a higher  $\Delta\chi^2_{\text{SNIa}+d_M}$ . The median values  $\Omega_{k,0}^{\text{med}}$  of the maximum likelihoods are recapitulated in Table 1 together with the median standard deviation  $\sigma_{\Omega_{k,0}^{\text{med}}}$  and the total spread  $\Delta\Omega_{k,0}$ .

Changing the selection criterion to  $\Delta\chi^2_{\text{SNIa}+d_M} < 0$ , we display the resulting  $\mathcal{O}_k$  diagnostic in Figure 7. We saw in section 3.1 that adding transverse BAO information to the  $\chi^2$  selection leads to a significant reduction in the number of selected reconstructions for the combination of Pantheon+ & DESI DR2 data. The curved patterns of the  $\mathcal{O}_k$  points at  $z = 1.32$  and  $z = 1.48$  in the Pantheon+ & DESI DR2 case are artefacts of the evolution  $\Delta\chi^2_{\text{SNIa}+d_M}$  with iterations (in red in the left panel of Fig. 3). The decrease and further increase in  $\Delta\chi^2_{\text{SNIa}+d_M}$  as the value of  $\mathcal{O}_k$  comes closer to the one favoured by SNIa data create the curved shape of the data points, which are ordered from left to right by decreasing  $\Delta\chi^2_{\text{SNIa}+d_M}$ . Indeed, we can see that the reconstructions significantly deviating from constant in the top row of Fig. 5 are absent from Fig. 7, and under selection criterion  $\Delta\chi^2_{\text{SNIa}+d_M} < 0$ , 82.34% of the remaining reconstructions from Pantheon+ & DESI DR2 pass the  $p$ -value test, i.e. are consistent with the FRLW metric. The median value of the  $\mathcal{O}_k$  diagnostic is  $\Omega_{k,0}^{\text{med}} = 0.033_{-0.072}^{+0.047} \pm 0.037$  (see Table 1), and the highest deviation from flatness is  $2.06\sigma$ . The preference for positive curvature remains.

In Pantheon+ & DESI DR2 low- $z$  data, for which 100% of reconstruction are consistent with FLRW, the median is  $\Omega_{k,0}^{\text{med}} = 0.091_{-0.131}^{+0.055} \pm 0.063$ . In this case, and unlike the  $\Delta\chi^2_{\text{SNIa}}$  selection, the calculation of  $\Delta\chi^2_{\text{SNIa}+d_M}$  was carried over three BAO measurements instead of five. Although the high redshift DESI data have been truncated, the reconstructions have still been smoothed on the full redshift range over the Pantheon+ dataset, keeping the SNIa part of  $\chi^2_{\text{SNIa}+d_M}$  unchanged. This restriction of the BAO data to the 3 lowest redshift bin ( $z \lesssim 1$ )

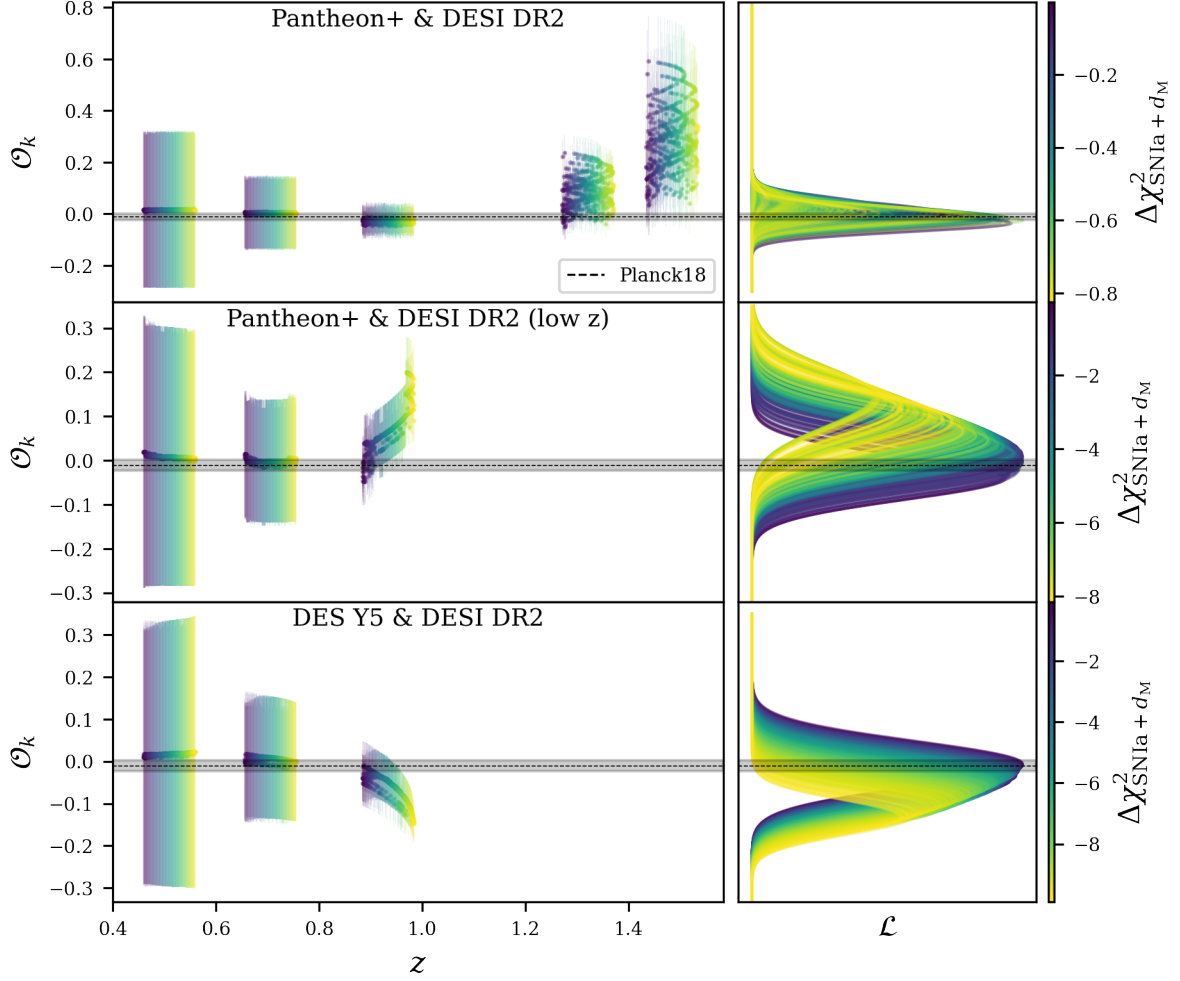


**Figure 7:** Results for the  $\mathcal{O}_k$  diagnostic, with selection criterion is  $\Delta\chi^2_{\text{SNIa}+d_M} < 0$ . On the right column are the likelihoods of each reconstruction, colour-coded by  $\Delta\chi^2_{\text{SNIa}+d_M}$ .

affects the value of  $\Delta\chi^2_{\text{SNIa}+d_M}$ , and therefore the selection itself. Some of the Pantheon+ reconstructions that did not meet the selection criterion  $\Delta\chi^2_{\text{SNIa}+d_M} < 0$  when considering all 5 BAO points are accepted once the high redshift data are removed. These additional reconstructions drive the estimation of  $\Omega_{k,0}^{\text{med}}$  toward a higher positive value. The highest deviation from flatness being  $2.13\sigma$ .

Unlike Pantheon+ & DESI DR2, DES Y5 & DESI DR2 are in better agreement with each other : the transition from the bottom row of Figure 5 to the bottom row of 7 does not significantly reduce the selection of reconstructions. We can see in Table 1 that  $\Omega_{k,0}^{\text{med}} = -0.119^{+0.113}_{-0.047} \pm 0.043$ , remains virtually unaffected by the change of selection criterion, as well as the  $-4.44\sigma$  maximum deviation from flatness. The conclusions for DES Y5 & DESI DR2 remain unchanged: FLRW is not ruled out, a negative curvature is still preferred, and most reconstructions are consistent with  $\Omega_{k,0} = 0$  within  $3\sigma$  (see middle panel of Fig. 6), except for those fitting the SNIa data the closest.

The last selection criterion :  $\Delta\chi^2_{\text{tot}} < 0$ , filters out most reconstructions inconsistent with flatness. The resulting collection is formed of reconstructions consistent with a flat

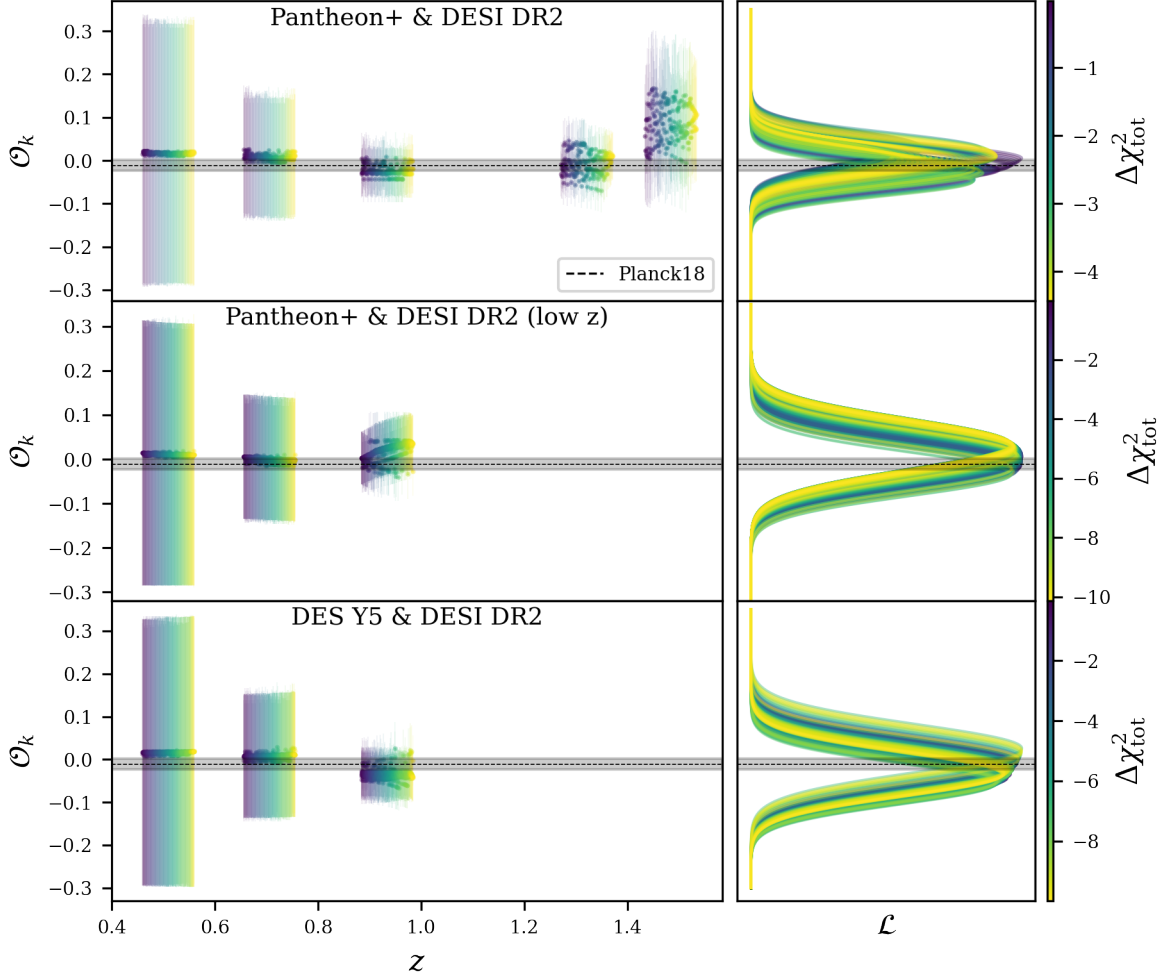


**Figure 8:** Results for the  $\mathcal{O}_k$  diagnostic, with selection criterion is  $\Delta\chi^2_{\text{tot}} < 0$ . On the right column are the likelihoods of each reconstruction, colour-coded by  $\Delta\chi^2_{\text{tot}}$ .

Universe, and should not be relied upon to perform a litmus test of FLRW and flatness, but is a good consistency check. As expected, adding the fit to the radial mode of the BAO in the selection criterion results in a significant trim for both data combination, and the remaining reconstructions are highly consistent with flatness:  $\Omega_{k,0}^{\text{med}} = -0.005^{+0.038}_{-0.045} \pm 0.036$  for Pantheon+ & DESI DR2,  $\Omega_{k,0}^{\text{med}} = 0.019^{+0.016}_{-0.056} \pm 0.056$  for the same data combination cut a low- $z$ , and  $\Omega_{k,0}^{\text{med}} = -0.030^{+0.056}_{-0.028} \pm 0.052$  for DES Y5 & DESI DR2. We see in the right panel of Fig. 6 that none deviate from flatness for more than  $1.5\sigma$  in absolute value.

#### 4 Discussion and conclusion

We performed a model-independent litmus test of the FLRW metric and the flatness of the universe. Using an iterative smoothing algorithm on Pantheon+ and DES Y5 data, we reconstructed  $\mathcal{D}(z)$  and  $\mathcal{D}'(z)$ . Then we evaluated these quantities at the redshifts of the BAO data from DESI DR2 and combined them with the transverse and radial modes  $d_M/r_d$  and  $d_H/r_d$  to obtain the  $\mathcal{O}_k$  diagnostic (eq. 2.1a & 2.3), a litmus test for both the FLRW metric and flatness.

$\Delta\chi^2$ criterion	Data combination	$\Omega_{k,0}^{\text{med}}$	$\frac{c}{H_0 r_d}$
$\Delta\chi^2_{\text{SNIa}} < 0$	P+ & DESI DR2	$0.058^{+0.043}_{-0.107} \pm 0.038$	$29.941^{+0.175}_{-0.007} \pm 0.140$
	P+ & DESI DR2 (low- $z$ )	$0.098^{+0.048}_{-0.134} \pm 0.064$	$30.219^{+0.034}_{-0.193} \pm 0.158$
	DES Y5 & DESI DR2	$-0.119^{+0.125}_{-0.047} \pm 0.043$	$30.781^{+0.019}_{-0.465} \pm 0.161$
$\Delta\chi^2_{\text{SNIa}+d_M} < 0$	P+ & DESI DR2	$0.033^{+0.047}_{-0.072} \pm 0.037$	$30.076^{+0.179}_{-0.099} \pm 0.141$
	P+ & DESI DR2 (low- $z$ )	$0.091^{+0.055}_{-0.131} \pm 0.063$	$30.217^{+0.218}_{-0.355} \pm 0.158$
	DES Y5 & DESI DR2	$-0.119^{+0.113}_{-0.047} \pm 0.043$	$30.781^{+0.123}_{-0.459} \pm 0.161$
$\Delta\chi^2_{\text{tot}} < 0$	P+ & DESI DR2	$-0.005^{+0.038}_{-0.045} \pm 0.036$	$30.044^{+0.528}_{-0.325} \pm 0.141$
	P+ & DESI DR2 (low- $z$ )	$0.019^{+0.016}_{-0.056} \pm 0.056$	$30.182^{+0.594}_{-0.524} \pm 0.158$
	DES Y5 & DESI DR2	$-0.030^{+0.056}_{-0.028} \pm 0.052$	$30.486^{+0.274}_{-0.460} \pm 0.160$

**Table 1:** Recap table of  $\Omega_{k,0}^{\text{med}}$ , along with the spread of all reconstructions and the median  $1\sigma$  error, and of median value of  $c/(H_0 r_d)$  with  $1\sigma$  error, for each data combination and each  $\Delta\chi^2$  selection criterion. Results were calculated using only the reconstructions consistent with the FLRW metric with 95% confidence.

For the Pantheon+ & DESI DR2 data combination, the reconstructed  $\mathcal{O}_k$  diagnostics, because they present a deviation from constant at high-redshift, are for the most part inconsistent with the FLRW metric. The closer the reconstructions are to the (SN) data, the more important this deviation is. Only 1.11% of reconstructions do not rule out the FLRW metric, and these few reconstructions are also consistent with flatness within  $3\sigma$ , with a preference for positive curvature. However, when considering the fit to the transverse mode of the BAO  $d_M/r_d$ , the reconstructions excluding the FLRW metric are rejected by the selection criterion  $\Delta\chi^2_{\text{SNIa}+d_M} < 0$ , showing an inconsistency between the Pantheon+ SNIa and the DESI DR2 BAO. Under this new criterion, 100% of the selected reconstructions are consistent with FLRW, and most are also consistent with flatness within  $3\sigma$ , but some of the best fitting reconstructions show a  $> 3\sigma$  deviation from flatness. When restricting the redshift range to  $z < 1.13$  (i.e. the BAO datapoints with the two highest redshifts are removed from the DESI DR2 data), the reconstructed distances from SNIa and the BAO transverse distances become fully consistent with an FLRW universe, supporting that the tension with the FLRW metric is driven by the high-redshift end of the Pantheon+ SNIa, where the data are sparse and less reliable. Supernovae with  $z > 1$  have typically larger systematic uncertainties due to selection effects such as the Malmquist bias. A study of the Pantheon dataset [23] showed that a simple linear correction for Malmquist bias efficiently reduces deviations in the high-redshift reconstructions, although this correction is not statistically required by the data. Similarly, the high-redshift BAO data points removed in this part of the analysis are those most affected by modeling and systematic uncertainties [24].

The DES Y5 SNIa data do not show such tension with the DESI DR2 BAO data. The selection of reconstructions is barely affected by the change in the selection criterion from  $\Delta\chi^2_{\text{SNIa}} < 0$  to  $\Delta\chi^2_{\text{SNIa}+d_M} < 0$ , indicating good agreement between the two data sets. In both cases, the reconstructed  $\mathcal{O}_k$  diagnostic does not rule out the FLRW metric, and most of

them are consistent with flatness within  $3\sigma$ .

Finally, the use of  $\Delta\chi_{\text{tot}}^2 < 0$  as the selection criterion supports the fact that the use of the  $\mathcal{O}_k$  diagnostic as a test for  $\Omega_{k,0}$  is reliable, since we recover an  $\mathcal{O}_k$  diagnostic highly consistent with  $\Omega_{k,0} = 0$  (within  $1.5\sigma$ ) for all combination of data, and this after biasing the collection of selected reconstructions toward flatness.

Our results are consistent with the Planck 2018 [3] results, and with previous model-independent tests of the FLRW metric involving SNIa and BAO data, which are in agreement with FLRW and flatness. Slight preference for various sign of  $\Omega_{k,0}$  appears depending on the data combination and the method, but these preference are never statistically significant. In [12], negative curvature is slightly favoured, while in [14] (Strong lensing sources and the Pantheon compilation), the same is true for positive curvature ( $\Omega_{k,0} = 0.12^{+0.27}_{-0.25}$ ). Similarly, null-test of the FLRW metric with Pantheon+ SNIa and DESI DR2 BAO found no deviation from FLRW, and no strong evidence for curvature within the FLRW metric [13]. As for tests of spatial curvature only, they usually find no significant deviation from flatness. Pantheon+ SNIa combined to Cosmic Chronometers (CCH) in [25] give  $\Omega_{k,0} = -0.02 \pm 0.14$ , in [26] DES Y5 & DESI DR2 combined with CCH resulted in  $\Omega_{k,0} = -0.143 \pm 0.085$  ( $1.7\sigma$  deviation from flatness) and  $\Omega_{k,0} = -0.107^{+0.079}_{-0.085}$  when replacing the DES Y5 data by Pantheon+, and combined to Fast Radio Bursts in [27] the DESI DR2 data indicate  $\Omega_{k,0} = -0.09^{+0.24}_{-0.31}$ .

Since high redshift Pantheon+ SNIa data revealed themselves to be quite unreliable for model-independent reconstructions of the expansion history, the robustness of the  $\mathcal{O}_k$  diagnostic is confined to the low-redshift regime. To extend this model independent test of the FLRW metric and spatial curvature, we will require better high SNIa observations, or alternative cosmological probes with reliable data above  $z \gtrsim 1$ . Standard sirens are promising candidates for future tests, especially the upcoming third generation of ground based detector [28]. Generated mock data of upcoming Gravitational Waves survey going up to redshift  $z \sim 5$  result in a significant improvement of the constraints on cosmological parameters [29]. If these improvements remain highly model-dependent, standard sirens can also meet, and even exceed the constraint on  $\Omega_{k,0}$  from DES in a model independent framework [30].

It is important to note that the results of this work depend on the choice of the smoothing scale  $\Delta = 0.3$ . Alternative results of the analysis with  $\Delta = 0.2$  and  $\Delta = 0.4$  are available in Appendix A. A lower smoothing scale tends to fit the data closely and reinforces the preferences of the datasets for positive or negative values of  $\Omega_{k,0}$ . On the contrary, a higher smoothing scale ( $\Delta = 0.4$ ) results in reconstruction less affected by the particularities of each dataset, and the resulting  $\mathcal{O}_k$  diagnostic present a stronger agreement both with flatness and other datasets. The value  $\Delta = 0.3$  was used in various studies involving different SNIa compilations such as the Joint Light-curve Analysis [9] (740 SNIa), the Pantheon sample [10] (1048 SNIa) or mock LSST data [11] (14 bins). Since the optimal value of  $\Delta$  depends on the size and the quality of the sample, it seems relevant to re-evaluate the optimal value of  $\Delta$  specifically for the Pantheon+ and DES Y5 compilations in future studies. Alternatively, we could also implement a dynamical smoothing scale  $\Delta(z)$ , as has already been suggested in [17]. The latter option seems to be particularly interesting given the important impact that the sparsity of the high- $z$  Pantheon+ data appears to have on our results.

## A Smoothing scale

Table A.1 recapitulates the results of the  $\mathcal{O}_k$  diagnostic after re-running the full pipeline with smoothing scale  $\Delta = 0.2$  and  $\Delta = 0.4$ . The corresponding deviation histograms are in the

$\Delta\chi^2$ criterion	Data combination	$\Delta = 0.2$	$\Delta = 0.4$
$\Delta\chi^2_{\text{SNIa}} < 0$	P+ & DESI DR2	$0.072^{+0.040}_{-0.105} \pm 0.038$	$0.085^{+0.036}_{-0.135} \pm 0.039$
	P+ & DESI DR2 (low-z)	$0.300^{+0.005}_{-0.335} \pm 0.082$	$0.011^{+0.005}_{-0.047} \pm 0.054$
	DES Y5 & DESI DR2	$-0.176^{+0.174}_{-0.043} \pm 0.037$	$-0.066^{+0.072}_{-0.061} \pm 0.048$
$\Delta\chi^2_{\text{SNIa}+d_M} < 0$	P+ & DESI DR2	$0.041^{+0.044}_{-0.074} \pm 0.037$	$0.027^{+0.041}_{-0.064} \pm 0.037$
	P+ & DESI DR2 (low-z)	$0.172^{+0.066}_{-0.207} \pm 0.071$	$0.011^{+0.005}_{-0.049} \pm 0.054$
	DES Y5 & DESI DR2	$-0.176^{+0.162}_{-0.043} \pm 0.037$	$-0.066^{+0.063}_{-0.061} \pm 0.048$
$\Delta\chi^2_{\text{tot}} < 0$	P+ & DESI DR2	$0.000^{+0.014}_{-0.033} \pm 0.035$	$0.002^{+0.036}_{-0.052} \pm 0.036$
	P+ & DESI DR2 (low-z)	$0.005^{+0.033}_{-0.040} \pm 0.054$	$0.011^{+0.016}_{-0.047} \pm 0.054$
	DES Y5 & DESI DR2	$-0.032^{+0.047}_{-0.024} \pm 0.051$	$-0.025^{+0.042}_{-0.034} \pm 0.052$

**Table A.1:** Results of the  $\mathcal{O}_k$  diagnostic for different values of the smoothing scale  $\Delta$

displayed in the top and bottom rows of Fig. A.1 respectively.

With  $\Delta = 0.2$ , the smoothing is more sensitive to the noise and variations in the data. The peaks of the histograms in the top panel of Fig. A.1 are displaced toward stronger deviation compared to Fig. 6, showing that the preference for negative curvature in DES Y5, and positive curvature in Pantheon+ have been reinforced by the smaller smoothing scale. In this case, the reconstructions from Pantheon+ & DESI DR2 (low-z) deviates more significantly from flatness than Pantheon+ & DESI DR2, which is not the case for higher values of  $\Delta$ . The Pantheon+ data become significantly sparser around  $z \sim 1$ , and the reduction of the value of the smoothing scale generate stronger deviations toward positive values in the  $\mathcal{O}_k$  diagnostic reconstructions at  $z = 1.13$ , the maximum redshift of Pantheon+ & DESI DR2 (low-z), and drive the peak of the histogram (in orange) toward high, positive values. Meanwhile, the two higher redshift data points, present in the Pantheon+ & DESI DR2 data combination (in blue) deviate into negative value, explaining the final weighted average to be closer to  $\mathcal{O}_k = 0$  in this case.

With  $\Delta = 0.4$ , the reconstructions are smoother and SNIa that strongly deviate from the rest of the sample have less impact on the results. As a results, we can see in the bottom panel of Fig. A.1 that all reconstructions consistent with FLRW are also consistent with flatness within  $2.5\sigma$  in absolute value. The previous preferences for different values of  $\Omega_{k,0}$  remain, but the higher smoothing scale attenuates the disagreement between dataset and increases the consistency with flatness.

## Acknowledgments

This work was partially supported by the ‘‘PHC STAR’’ program (project number: 50123WB, RS-2023-00259422), funded by the French Ministry for Europe and Foreign Affairs, the French Ministry for Higher Education and Research, and the National Research Foundation of Korea. C. M. acknowledges the support of the Center for the Gravitational Waves Universe (grant number: 2021M3F7A1082056), B. L. acknowledges the support of the National Research Foundation of Korea (NRF-2022R1F1A1076338) and the support of the Korea Institute for Advanced Study (KIAS) grant funded by the government of Korea.

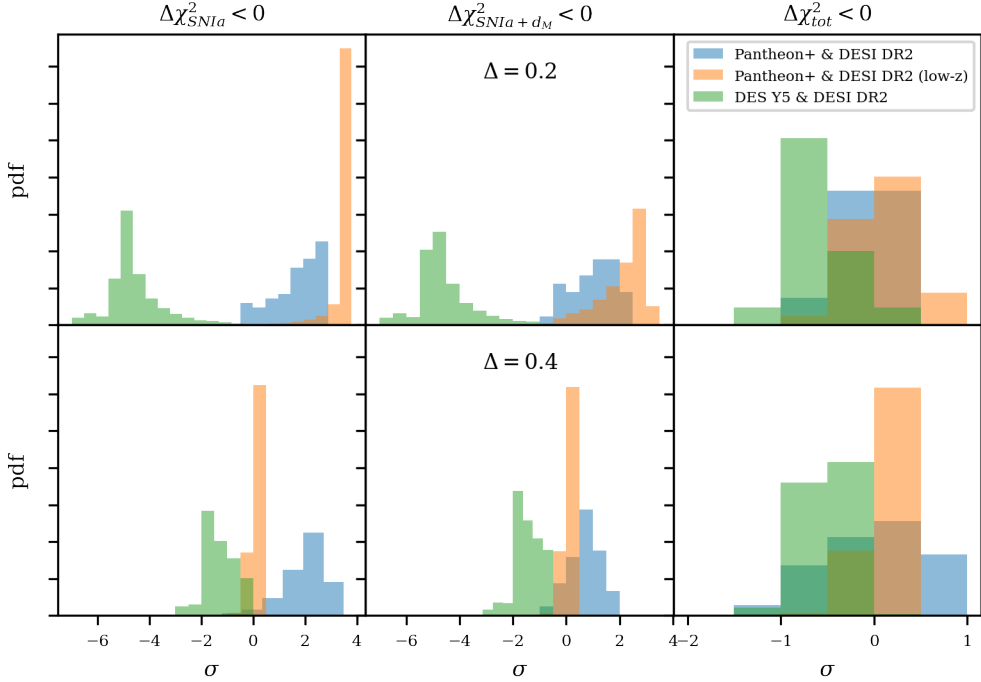


**Figure A.1:** Histogram of the deviations from flatness for  $\Delta = 0.2$  (top panel) and  $\Delta = 0.4$  (bottom panel).

## References

- [1] A.G. Riess, A.V. Filippenko, P. Challis, A. Clocchiatti, A. Diercks, P.M. Garnavich et al., *Observational evidence from supernovae for an accelerating universe and a cosmological constant*, *The Astronomical Journal* **116** (1998) 1009–1038.
- [2] S. Perlmutter, G. Aldering, G. Goldhaber, R.A. Knop, P. Nugent, P.G. Castro et al., *Measurements of  $\omega$  and  $\lambda$  from 42 high-redshift supernovae*, *The Astrophysical Journal* **517** (1999) 565–586.
- [3] Planck Collaboration, N. Aghanim, Y. Akrami, M. Ashdown, J. Aumont, C. Baccigalupi et al., *Planck 2018 results. VI. Cosmological parameters*, *A&A* **641** (2020) A6 [[1807.06209](#)].
- [4] DESI Collaboration, M. Abdul-Karim, J. Aguilar, S. Ahlen, S. Alam, L. Allen et al., *DESI DR2 Results II: Measurements of Baryon Acoustic Oscillations and Cosmological Constraints*, *arXiv e-prints* (2025) [arXiv:2503.14738](#) [[2503.14738](#)].
- [5] E. Di Valentino, J.L. Said, A. Riess, A. Pollo, V. Poulin, A. Gómez-Valent et al., *The cosmoverse white paper: Addressing observational tensions in cosmology with systematics and fundamental physics*, *Physics of the Dark Universe* **49** (2025) 101965.
- [6] E. Di Valentino, O. Mena, S. Pan, L. Visinelli, W. Yang, A. Melchiorri et al., *In the realm of the Hubble tension-a review of solutions*, *Classical and Quantum Gravity* **38** (2021) 153001 [[2103.01183](#)].
- [7] C. Clarkson, B. Bassett and T.H.-C. Lu, *A General Test of the Copernican Principle*, *Phys. Rev. Lett.* **101** (2008) 011301 [[0712.3457](#)].
- [8] A. Shafieloo and C. Clarkson, *Model independent tests of the standard cosmological model*, *Phys. Rev. D* **81** (2010) 083537 [[0911.4858](#)].
- [9] B. L’Huillier and A. Shafieloo, *Model-independent test of the FLRW metric, the flatness of the*

*Universe, and non-local estimation of  $H_0$   $r_d$ , *J. Cosmology Astropart. Phys.* **2017** (2017) 015* [[1606.06832](#)].

- [10] A. Shafieloo, B. L’Huillier and A.A. Starobinsky, *Falsifying  $\Lambda$  CDM : Model-independent tests of the concordance model with eBOSS DR14Q and Pantheon*, *Phys. Rev. D* **98** (2018) 083526 [[1804.04320](#)].
- [11] B. L’Huillier, A. Mitra, A. Shafieloo, R.E. Keeley and H. Koo, *Litmus tests of the flat  $\Lambda$ CDM model and model-independent measurement of  $H_0$   $r_d$  with LSST and DESI*, *J. Cosmology Astropart. Phys.* **2025** (2025) 030 [[2407.07847](#)].
- [12] F. Montanari and S. Räsänen, *Backreaction and  $frw$  consistency conditions*, *Journal of Cosmology and Astroparticle Physics* **2017** (2017) 032–032.
- [13] B.R. Dinda, R. Maartens, S. Saito and C. Clarkson, *Improved null tests of  $\lambda$ cdm and  $flrw$  in light of desi dr2*, *Journal of Cosmology and Astroparticle Physics* **2025** (2025) 018.
- [14] T. Collett, F. Montanari and S. Räsänen, *Model-Independent Determination of  $H_0$  and  $\Omega_{K0}$  from Strong Lensing and Type Ia Supernovae*, *Phys. Rev. Lett.* **123** (2019) 231101 [[1905.09781](#)].
- [15] D. Scolnic, D. Brout, A. Carr, A.G. Riess, T.M. Davis, A. Dwomoh et al., *The Pantheon+ Analysis: The Full Data Set and Light-curve Release*, *ApJ* **938** (2022) 113 [[2112.03863](#)].
- [16] DES collaboration, *The dark energy survey: Cosmology results with 1500 new high-redshift type ia supernovae using the full 5 yr data set*, *The Astrophysical Journal Letters* **973** (2024) L14.
- [17] A. Shafieloo, U. Alam, V. Sahni and A.A. Starobinsky, *Smoothing supernova data to reconstruct the expansion history of the Universe and its age*, *MNRAS* **366** (2006) 1081 [[astro-ph/0505329](#)].
- [18] A. Shafieloo, *Model-independent reconstruction of the expansion history of the Universe and the properties of dark energy*, *MNRAS* **380** (2007) 1573 [[astro-ph/0703034](#)].
- [19] B. L’Huillier, A. Shafieloo and H. Kim, *Model-independent cosmological constraints from growth and expansion*, *MNRAS* **476** (2018) 3263 [[1712.04865](#)].
- [20] H. Koo, A. Shafieloo, R.E. Keeley and B. L’Huillier, *Model-independent Constraints on Type Ia Supernova Light-curve Hyperparameters and Reconstructions of the Expansion History of the Universe*, *ApJ* **899** (2020) 9 [[2001.10887](#)].
- [21] H. Koo, A. Shafieloo, R.E. Keeley and B. L’Huillier, *Model selection and parameter estimation using the iterative smoothing method*, *J. Cosmology Astropart. Phys.* **2021** (2021) 034 [[2009.12045](#)].
- [22] H. Koo, R.E. Keeley, A. Shafieloo and B. L’Huillier, *Bayesian vs frequentist: comparing Bayesian model selection with a frequentist approach using the iterative smoothing method*, *J. Cosmology Astropart. Phys.* **2022** (2022) 047 [[2110.10977](#)].
- [23] B. L’Huillier, A. Shafieloo, E.V. Linder and A.G. Kim, *Model independent expansion history from supernovae: Cosmology versus systematics*, *MNRAS* **485** (2019) 2783 [[1812.03623](#)].
- [24] M. Abdul Karim, J. Aguilar, S. Ahlen, S. Alam, L. Allen, C.A. Prieto et al., *Desi dr2 results. ii. measurements of baryon acoustic oscillations and cosmological constraints*, *Physical Review D* **112** (2025) .
- [25] Y. Liu, S. Cao, T. Liu, X. Li, S. Geng, Y. Lian et al., *Model-independent constraints on cosmic curvature: Implication from updated hubble diagram of high-redshift standard candles*, *The Astrophysical Journal* **901** (2020) 129.
- [26] A. Favale, A. Gómez-Valent and M. Migliaccio, *Revisiting model-independent constraints on spatial curvature and cosmic ladders calibration: updated and forecast analyses*, *arXiv e-prints* (2025) arXiv:2511.19332 [[2511.19332](#)].

- [27] J.A.S. Fortunato, W.S. Hipólito-Ricaldi and G.E. Romero, *Probing Cosmic Curvature with Fast Radio Bursts and DESI DR2*, *arXiv e-prints* (2025) arXiv:2506.01504 [[2506.01504](https://arxiv.org/abs/2506.01504)].
- [28] S. Cao, J. Qi, Z. Cao, M. Biesiada, J. Li, Y. Pan et al., *Direct test of the FLRW metric from strongly lensed gravitational wave observations*, *Scientific Reports* **9** (2019) 11608 [[1910.10365](https://arxiv.org/abs/1910.10365)].
- [29] F.B. Medeiros dos Santos, J. Morais, S. Pan, W. Yang and E. Di Valentino, *A New Window on Dynamical Dark Energy: Combining DESI-DR2 BAO with future Gravitational Wave Observations*, *arXiv e-prints* (2025) arXiv:2504.04646 [[2504.04646](https://arxiv.org/abs/2504.04646)].
- [30] K. Liao, *Constraints on cosmic curvature with lensing time delays and gravitational waves*, *Phys. Rev. D* **99** (2019) 083514 [[1904.01744](https://arxiv.org/abs/1904.01744)].